AGU PUBLICATIONS

Water Resources Research

RESEARCH ARTICLE

10.1002/2013WR014374

Key Points:
- Linking flood frequency curve to annual water balance by analyzing MOPEX data set
- Aridity index has a first-order control on mean and C_v of annual maximum floods
- Base flow index is secondary control on shape/magnitude of flood frequency curve

Correspondence to:
H.-Y. Li,
Hongyi.li@pnnl.gov

Citation:
Guo, J., H.-Y. Li, L. R. Leung, S. Guo, P. Liu, and M. Sivapalan (2014), Links between flood frequency and annual water balance behaviors: A basis for similarity and regionalization, *Water Resour. Res.*, *50*, doi:10.1002/2013WR014374.

Received 3 JULY 2013
Accepted 17 JAN 2014
Accepted article online 22 JAN 2014

Links between flood frequency and annual water balance behaviors: A basis for similarity and regionalization

Jiali Guo[1,2], Hong-Yi Li[2], L. Ruby Leung[2], Shenglian Guo[1], Pan Liu[1], and Murugesu Sivapalan[3,4]

[1]State Key Laboratory of Water Resources and Hydropower Engineering Science, Wuhan University, Wuhan, Hubei, China, [2]Pacific Northwest National Laboratory, Richland, Washington, USA, [3]Department of Civil and Environmental Engineering, Hydrosystems Laboratory, University of Illinois at Urbana-Champaign, Urbana, Illinois, USA, [4]Department of Geography and Geographic Information Science, University of Illinois at Urbana-Champaign, Urbana, Illinois, USA

Abstract This paper presents the results of a data-based comparative study of several hundred catchments across continental United States belonging to the MOPEX data set to systematically explore the connection between the flood frequency curve and mean annual water balance. Mean annual water balance is expressed in terms of two similarity measures: (i) the climatic aridity index, *AI*, which is a measure of the competition between energy and water availability and (ii) the base flow index, *BFI*, which is a measure of total runoff partitioning into surface and subsurface components at the annual time scale. The data analyses showed that the aridity index, *AI*, has a first-order control on the shape of the flood frequency curve (also known as the growth curve), as expressed in terms of both the *mean* and *coefficient of variation* (C_v) of the annual maximum floods, once normalized by catchment size (i.e., specific flood discharge) While the mean annual (specific) flood discharge decreases with increasing aridity, C_v increases with increasing aridity. On the other hand, the *BFI* was found to be a second-order control on the flood frequency curve. Higher *BFI*, meaning higher contributions of subsurface flow to total streamflow, leads to a decrease of the mean annual (specific) flood discharge, and vice versa. The statistically significant relationship between *AI* and the flood frequency curve and the consistent shift of the growth curves with *AI* support the use of *AI* as a similarity measure for regionalization of flood frequency.

1. Introduction

Flooding is one of the major water-related natural hazards with significant societal, economic, hydrological, and ecological consequences. Estimation and/or prediction of floods is, therefore, necessary for flood mitigation. Statistical approaches to flood estimation (e.g., flood frequency curve (FFC)) have been practiced extensively for about a century since *Fuller* [1914]. There have been many improvements along the way but most of the flood estimation methods practiced today still rely on the same fundamental statistical principles. These statistical methods for flood frequency analysis estimate FFC statistics mainly based on historical records at well-gauged locations. Such estimates are not easily transferable from well-gauged to poorly or ungauged sites, nor to future conditions [*Struthers and Sivapalan*, 2007]. Sufficiently long records of streamflow observations required for such estimation are simply not available over major portions of the global domain.

One of the common approaches used to estimate flood frequencies in ungauged sites is through extrapolation from well-gauged to poorly gauged or ungauged sites. This is generally known as "regionalization," which is carried out on the basis of "flood frequency similarity." In this case, hydrologically homogeneous regions within which the flood frequency curves show a similarity of functional form or shape are identified, and the parameters of the appropriate flood frequency distributions are extrapolated to ungauged locations through statistical regressions against climatic and landscape characteristics, such as mean annual precipitation ($\bar{P}$), catchment area, soils, geology, etc. [*Rosbjerg et al*., 2013]. In this case, both the notion of similarity and regionalization are statistical, i.e., they are not necessarily founded on understanding of processes contributing to flood frequency.

As climate changes in the future may lead to more frequent extreme climate events (e.g., heat waves, extreme rainstorms, etc.) [*Leung et al*., 2003; *Tebaldi et al*., 2012], flood peaks derived from past historical records may not be representative of the present and future flood behavior. This issue is exacerbated

© 2014. American Geophysical Union. All Rights Reserved.

further by the impacts of direct anthropogenic activities such as land use/cover change (e.g., deforestation and urbanization) and impoundment by dams and reservoirs. Given the intrinsic weaknesses of conventional statistical approaches under these circumstances, more process-based understanding is called upon to shed light on the climatic and landscape controls shaping the FFC, including components such as runoff generation and runoff routing, and effects of human activities on these processes [*Merz and Blöschl*, 2008b, 2008c; *Rosbjerg et al*., 2013; *Viglione et al*., 2013]. The notion of hydrologic similarity is still relevant in this case, except that now the FFCs of two catchments are deemed similar if they arise from similar component hydrologic processes. Examples of process-based analysis of flood frequency similarity include *Wood and Hebson* [1986], *Sivapalan et al*. [1990], and *Robinson and Sivapalan* [1997a], all of which adopted a derived flood frequency approach, analyzing event-scale flood generation processes within a probabilistic framework.

There has been a long-felt need for a combination of statistical and process-based approaches to flood frequency estimation. On the statistical side, $\bar{P}$ has been widely and successfully used as a measure of climate similarity in flood frequency regionalization studies [*Madsen and Rosbjerg*, 1997; *Merz and Blöschl*, 2008b, 2008c; *Reed et al*., 1999, and references therein]. Likewise, *Merz and Blöschl* [2008a] demonstrated a connection between statistical moments of annual maximum floods and long-term water balance indicators such as $\bar{P}$ and the base flow index (*BFI*), which measures the partitioning of annual total runoff into fast and slow (i.e., base flow) components. The surprising usefulness of $\bar{P}$ for flood frequency regionalization, for example, may be attributed to several factors: (1) mean annual precipitation may indeed be correlated, within a hydrometeorological context, with the magnitudes of extreme rainfall events that cause large floods; (2) mean annual precipitation in an annual water balance context is an important factor that governs the regime of antecedent soil moistures that develops in a catchment, which in turn is an important control of flood magnitudes; and (3) mean annual precipitation as a climatic measure may be indicative or a control of those landscape properties (e.g., soil, vegetation, and topography) that determine the magnitude of flood peaks [*Rosbjerg et al*., 2013].

On the process side too, as early as 1976, *Wood* [1976] demonstrated the importance of antecedent soil moisture in derived flood frequency approaches. This was further confirmed by *Sivapalan et al*. [2005] who explicitly factored the role of seasonality on antecedent soil moisture, and in this way connected flood frequency with long-term seasonal water balance. Flood frequency has also been shown to be closely related to long-term water balance. Earlier, using a derived flood frequency approach, *Blöschl and Sivapalan* [1997] showed that the coefficient of variation (C_v) of annual maximum floods decreases with the *BFI*, the fraction of annual base flow to total flow. Apart from the fact that the connection can help improve regionalization of flood frequency, it also raises the deeper question: What is the nature of the connection between annual water balance and the flood frequency curve? Clearly, both are signatures of water balance variability, and both arise out of the complex process interactions and feedbacks that go on within a catchment. Whereas annual water balance is a signature of water balance variability at one end of the spectrum (i.e., annual time scale), the flood frequency curve represents variability at the opposite end of the spectrum (i.e., extremes at event scale).

The above discussion has motivated us to investigate the linkages between the flood frequency and annual water balance behaviors, as different signatures of hydrologic variability, in the hope that new understanding and the recent advances related to annual water balance could be easily transferred to, or shed light on, the investigation of regional flood frequency behavior. What is presented here is a purely empirical, data-based analysis of a large number of catchments across the contiguous United States. The goal is to try and draw connections in a top-down manner, and to provide some insights into these connections based purely on additional diagnostic data analysis, whereas a more process-based exploration of the connections will be addressed in future work. The rest of the paper is organized as follows. In section 2, we describe the data sources and the methodology used in this paper. Section 3 presents and interprets the empirical evidence of the linkages between regional flood frequency and annual water balance. Section 4 presents the main conclusions drawn from the analyses, and outlines possible future directions of research to consolidate the understanding gained from this empirical study.

2. Data and Methodology

2.1. Data

The work presented here involves a comparative study of several hundred catchments across the contiguous United States. The data used in this study are mostly taken from the Model Parameter Estimation

© 2014. American Geophysical Union. All Rights Reserved.

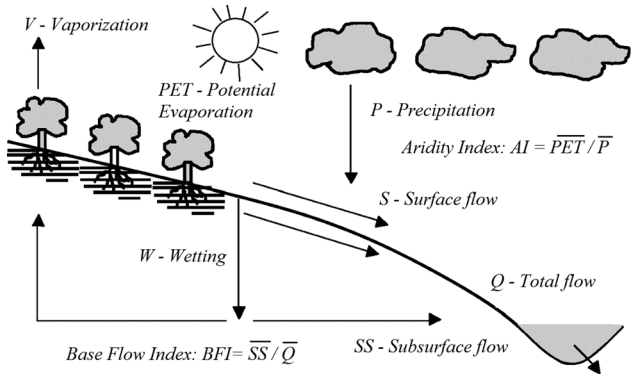

Figure 1. A conceptual model of annual hydrologic water balance partitioning at the land surface (modified after Figure 1 from *Sivapalan et al.* [2011]).

Experiment (MOPEX) data set [*Duan et al.*, 2005], downloadable from the webpages of the National Weather Service located within the National Oceanic and Atmospheric Administration (NOAA) (ftp://hydrology.nws.noaa.gov/pub/gcip/mopex/US_Data/). We use a subset of the MOPEX data set, including daily precipitation data, potential evapotranspiration, and streamflow covering the period from 1948 to 2003. These are used to generate both flood frequency curves (at the daily time scale) and various measures of annual water balance. As flood frequency analysis requires long data records, we selected 266 catchments (as shown in Figure 1) out of the original 438 MOPEX catchments by removing those with gaps in daily precipitation and potential evapotranspiration, and relatively large gaps in daily streamflow (i.e., more than 5 years). The drainage areas of the 266 selected study catchments range from 113 to 10,209 km^2. They span most major geological and climate regions within the contiguous United States, although there is a significant bias toward the wetter, more populous, less alpine, and more heavily monitored catchments in the eastern United States. In addition to the daily data from the MOPEX data set, for some of the analyses presented in the paper hourly precipitation data was also used and this data covered the same time period as the daily data.

2.2. Statistical Moments of Annual Maximum Flood

First of all, the FFCs studied in this paper are generated from the daily streamflow data, and may be different from FFCs that could be constructed on the basis of more fine-scale flow data, especially in some of the smaller catchments. Since the objective of this study is not flood frequency regionalization per se, but a scientific investigation of the links between flood frequency and annual water balance (both considered as signatures of streamflow variability), this is not considered a major drawback. Second, since the sizes of the study catchments cover a large range, to minimize the size effects, in this study we will only deal with specific annual floods, i.e., annual flood values divided by the corresponding catchment area. We are aware that even the use of specific annual floods may not overcome all size effects, such as those caused by the interplay between spatial heterogeneity of precipitation and landscape properties. We therefore limit our study focus to connections between flood frequency and annual water balance. Any scale effects that may manifest in this connection are left for future study.

In order to characterize the shape of the FFC, we will estimate the first two moments of the annual maximum floods: these are the specific mean annual maximum daily flow (Mean) and the coefficient of variation (C_v), respectively, which are estimated from the annual maximum daily streamflow obtained from the MOPEX database, as follows:

$$\text{Mean} = \frac{1}{n}\sum_{i=1}^{n} x_i \tag{1a}$$

$$\text{Std} = \sqrt{\frac{1}{n-1}\sum_{i=1}^{n}(x_i - \text{Mean})^2} \tag{1b}$$

$$C_v = \frac{\text{Std}}{\text{Mean}} \tag{1c}$$

where x_i is the observed specific annual maximum of daily streamflow in year i in mm/day and n is the number of years of record. As we shall see later, these estimates will be repeated for the surface (fast) and subsurface (slow) components of total streamflow as well.

© 2014. American Geophysical Union. All Rights Reserved.

In order to generate the FFCs the streamflow data are first arranged in descending order. Each data point is assigned a rank starting with 1. Many plotting-position formulae are available but they can all be expressed as special cases of

$$P(m)=\frac{m-a}{N+b} \text{ or } T(m)=\frac{N+b}{m-a} \tag{2}$$

where m is the mth ranked data, $P(m)$ is the exceedance probability of the mth ranked data (when annual maximum flood data is arranged in descending order), $T(m)$ is the corresponding return period, N is the length of record, and a and b are appropriate fitting parameters. In this study, we adopted the Gringorten plotting-position formula recommended by *Singh et al*. [2005], and the values of a and b are set as 0.44 and 0.12, respectively. Since the entire focus of this study is on understanding rather than prediction, the FFCs are derived directly from the observed flow data without fitting them to any statistical distribution: raw moments presented in equation (1) are used in the comparative analyses.

2.3. Annual Water Balance and Associated Similarity Indices

Figure 1 is a schematic that illustrates the two-stage annual water balance partitioning at the catchment scale [*L'vovich*, 1979; *Sivapalan et al*., 2011]. In Stage 1, annual precipitation P is partitioned into a surface (or fast) runoff component S and an infiltrated component, which is called wetting W. In Stage 2, catchment wetting W is in turn further partitioned into a subsurface (or slow) runoff component SS and an energy-dependent vaporization component (evaporation plus transpiration) V. The quick surface flow and slow subsurface flow components combine together to yield the total streamflow Q. This two-stage partitioning can be expressed as follows:

$$P=S+W \tag{3a}$$

$$W=SS+V \tag{3b}$$

The combined annual water balance, neglecting carryover of storage between consecutive years, can then be written as

$$P=V+Q \tag{4a}$$

$$Q=S+SS \tag{4b}$$

We utilized the available MOPEX data set to carry out this partitioning, by means of base flow separation analyses. Many previous studies have used graphical, analytical, and digital filtering techniques to extract base flow from total streamflow [*Arnold and Allen*, 1999; *Arnold et al*., 1995; *Lyne and Hollick*, 1979; *Nathan and McMahon*, 1990; *Szilagyi and Parlange*, 1998]. In this paper, the recursive digital filter method, as embedded in the BFLOW program *Arnold et al*. [1995], is adopted for base flow separation since it has also been applied to the MOPEX basins in previous studies [*Sivapalan et al*., 2011; *Voepel et al*., 2011; *Ye et al*., 2012]. Based on studies conducted in southern Australia, *Nathan and McMahon* [1990] showed the recursive filter method to be a stable, reproducible and objective method of continuous base flow separation. The 1 parameter recursive filter [*Arnold and Allen*, 1999; *Arnold et al*., 1995] is given by

$$DSS_i=aDSS_{i-1}+\frac{1-a}{2}(DQ_i+DQ_{i-1}) \tag{5a}$$

$$DSS_i < DQ_i \tag{5b}$$

where DQ_i and DSS_i are daily streamflow and subsurface flow, respectively; a is a filter parameter and is used to compute subsurface flow and surface runoff from time series of total streamflow. In this case, the value of the filter parameter, a, is set to 0.925. This filter is applied to the streamflow data twice, backward and forward in time, to obtain more precise estimation of the base flow, especially near the beginning of the time series. The base flow separation procedure is implemented to decompose the daily time series of

© 2014. American Geophysical Union. All Rights Reserved.

total streamflow into the corresponding time series of surface runoff, *S*, and subsurface runoff, *SS*. The daily time series is then aggregated to the annual scale for *P, PET, Q, S*, and *SS*, and these are then averaged to obtain the corresponding mean annual values as well. More details of this procedure are presented in *Sivapalan et al*. [2011].

The mean annual water balance for each catchment can be characterized in terms of two dimensionless ratios: $\bar{Q}/\bar{P}$ and $\overline{SS}/\bar{Q}$, both of which can be extracted from the MOPEX data set (the latter following the base flow separation). The first number, which is complementary to $\bar{E}/\bar{P}$ (i.e., $\bar{Q}/\bar{P}=1-\bar{E}/\bar{P}$), is a measure of the partitioning of mean annual precipitation into mean annual runoff and mean annual evapotranspiration. It has been extensively studied in the recent past in terms of the Budyko framework [*Budyko*, 1974]. Budyko's early work, supported by extensive work done subsequently on large populations of catchments around the world, including the MOPEX catchments [*Blöschl et al*., 2013; *Sivapalan et al*., 2011], has shown that $\bar{Q}/\bar{P}$ is highly correlated to the climatic aridity index, *AI*, given by

$$AI=\frac{\overline{PET}}{\bar{P}} \tag{6}$$

which is the ratio of mean annual potential evaporation, $\overline{PET}$, to mean annual precipitation, $\bar{P}$. Values of *AI* are estimated based on annual values of precipitation and potential evapotranspiration available for all catchments contained within the MOPEX data set. Catchments with *AI* less than unity are classified as wet (or humid) since actual evaporation is limited not by precipitation but rather by energy availability, and conversely, catchments with *AI* greater than unity are classified as dry (or arid). For this reason, in this paper, we will use *AI* as one measure of annual water balance similarity.

The second annual water balance measure is the base flow index (*BFI*) defined as

$$BFI=\frac{\overline{SS}}{\bar{Q}} \tag{7}$$

the ratio of mean annual subsurface flow, $\overline{SS}$, over mean annual total streamflow, $\bar{Q}$, which is a measure of the relative dominance of slow (subsurface) and fast (surface) flow pathways within the catchment. Several factors seem to control this ratio, the most dominant of which are geology and vegetation, and perhaps climate as well [*Bloomfield et al*., 2009; *Gebert et al*., 2007; *Haberlandt et al*., 2001; *Lacey and Grayson*, 1998; *Longobardi and Villani*, 2008], although these links are not well understood to be quantified in terms of measurable climatic and landscape characteristics. In this paper, we will use the *BFI* estimated from runoff data in the MOPEX catchments as the second measure of annual water balance.

3. Results and Discussion

3.1. Pattern of Statistical Moments of Floods Over MOPEX Basins

The spatial variations of the *mean* and C_v of the specific annual maximum floods (AMF) amongst the MOPEX catchments are presented in Figure 2, showing distinct regional patterns. The *mean AMF* values shown in Figure 2a vary from 0.36 to 103.51 mm/d: they are mostly high in coastal regions such as the Appalachians and Pacific Northwest, i.e., generally higher than 30 mm/d and even higher than 100 mm/d in some places. In the Midwest region *mean AMF* tends to be somewhat smaller, i.e., generally less than 5 mm/d, with some even less than 1 mm/d. The pattern of C_v values is complementary to the patterns of *mean AMF*, with larger C_v values found mostly in areas with low *mean AMF*. This complementary relationship between the spatial patterns of the *mean AMF* and C_v values has also been reported in previous studies by *Zaman et al*. [2012] for Australia, *Osterkamp and Friedman* [2000] for the American West, and *Farquharson et al*. [1992] for arid areas of the world. The nature of the regional patterns and coherence of the *mean* and C_v of *AMF* suggest that there may be an association with water balance. In the generally wet eastern and western coastal zones, *mean AMF* tends to be large while C_v tends to be small. In the drier regions, e.g., the Midwest, *mean AMF* tends to be smaller, while C_v values are generally larger. These observations prompt us to explore the relationship between flood frequency characteristics and hydroclimate, as measured by the aridity index, *AI*: the results of this analysis are presented next.

© 2014. American Geophysical Union. All Rights Reserved.

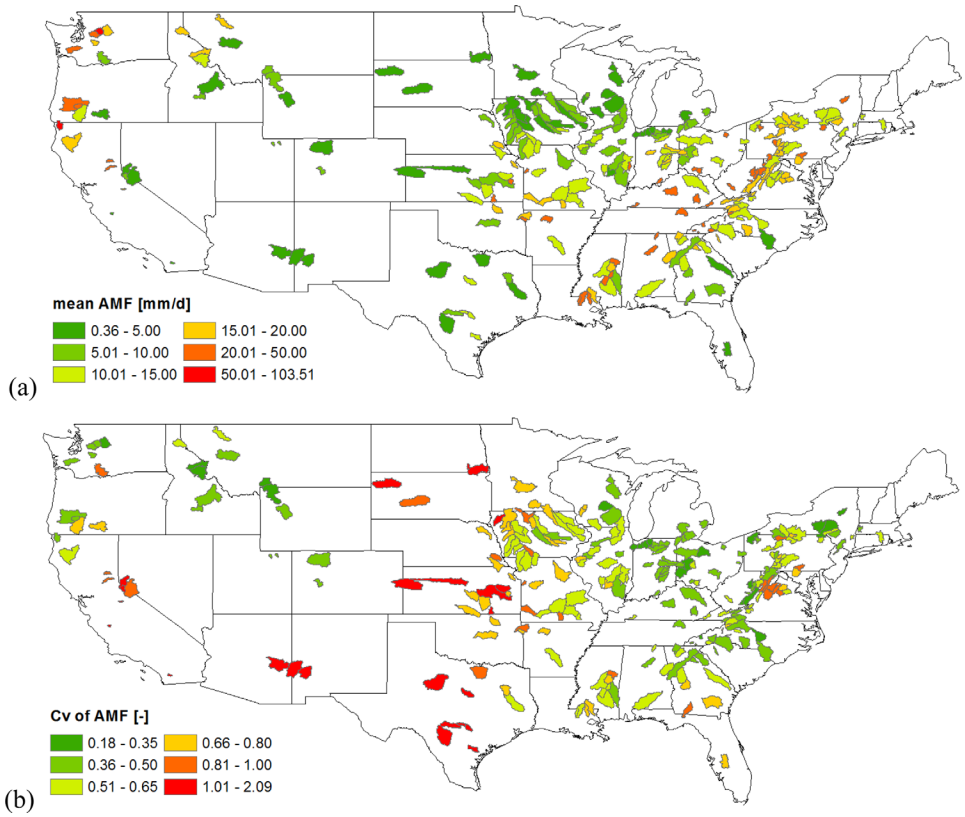

Figure 2. (a) Mean and (b) variability (coefficient of variation, C_v) of annual maximum flood over the 266 MOPEX basins used in the study.

3.2. Relationship Between AI and Annual Flood Statistics

Figure 3 shows the spatial distribution of mean annual precipitation, $\bar{P}$ and the aridity index, *AI*, for 266 MOPEX catchments. By comparing the results presented in Figures 2 and 3, one can find a striking resemblance between the patterns of *AI* values and those of *mean* and C_v of *AMF*. Indeed, there is an equally good association between $\bar{P}$ and the flood statistics: for reasons of brevity, these results are not presented here—from now onward the focus will be on the *AI*, because of its versatility in explaining many features of the catchment response, including flood response. An obvious spatial pattern exists showing that *AI* decreases from both the west and east coasts toward the inland parts of the United States. The most humid basins, with *AI* less than 0.6, are located in the Appalachian Mountains and Coastal mountains in the Pacific Northwest. Those MOPEX catchments with *AI* more than 2.0 are dominant in the Central Plains.

Motivated by these general observations, we generated scatterplots between *AI* and the two statistical moments of *AMF*, which are shown in Figure 4a (analogous plots against $\bar{P}$ are not presented for reason of brevity, but do indicate equally strong correlations). These scatterplots clearly show that there is close relationship between *AI* and the *AMF* statistics that determine the shape of the FFC. Overall, *mean AMF* decreases with increasing *AI* in a nonlinear way, whereas the C_v of *AMF* increases almost linearly with *AI*. We repeated the same analyses for flood frequency curves constructed for the annual maximum specific surface flow, S_{am}, and annual maximum subsurface flow, SS_{am}. We found similar relationships in these latter cases as well, except perhaps for a tighter relationship between the statistics of the annual maximum subsurface flow against *AI*. Given the relationship between *AI* and annual water balance, the same results can be presented in terms of the annual runoff coefficient (ratio of mean annual runoff to mean annual precipitation). These results are presented in Figure 4b, and equally significant relationships are obtained. A notable feature of Figure 4a is that the results stratified into four different classes based on catchment size, which shows that the relationship between flood frequency statistics and annual water balance (as measured by the aridity index) remains valid in spite of differences between size classes. This justifies the use of the flood frequency curve based on specific flood discharges as a signature of flood frequency similarity, in spite of using only daily streamflows for the construction of the flood frequency curves. The relationships

© 2014. American Geophysical Union. All Rights Reserved.

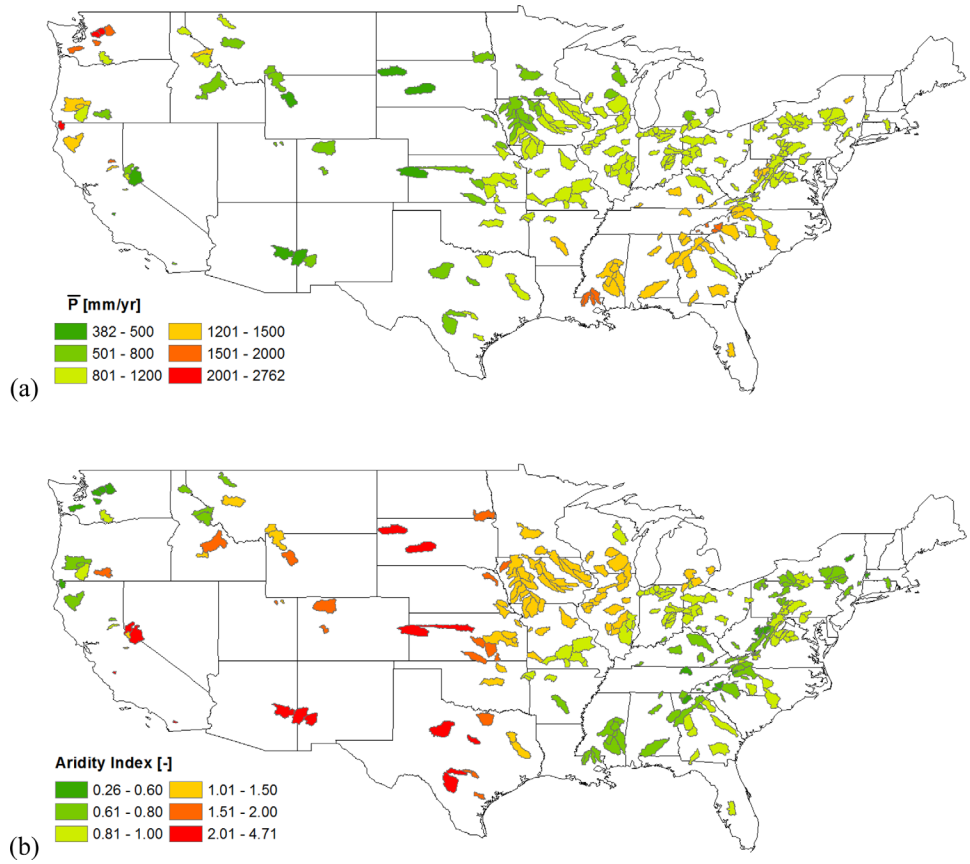

Figure 3. Spatial distribution of (a) mean annual precipitation ($\bar{P}$) and (b) the climatic aridity index (*AI*) for 266 MOPEX basins.

between annual water balance and AI (or annual runoff coefficient) can be fitted with linear or log-linear formulas as listed in Table 1. All the fitted formulas have pasted the significance test at 5% level, which confirms the statistical significance of the relationships described above.

The results presented in Figures 2–4 suggest that there is indeed a connection between flood frequency and annual water balance, and that *AI* is an important measure of the regional variations of the flood frequency curves. In order to better capture the effect of *AI* on the flood frequency curve, we next constructed a dimensionless flood frequency curve for each catchment, i.e., annual maximum flood values scaled by the mean annual flood. We next grouped all the 266 study catchments into six distinct classes on the basis of their *AI* values. Note that this analysis permits grouping of catchments having similar climates, but the catchments within each class are not necessarily contiguous. Assuming similarity within each class, the dimensionless flood frequency curves are then averaged (i.e., based on an arithmetic average of the dimensionless flood magnitudes for a given return period) to produce a characteristic, dimensionless flood frequency curve, or *growth curve*, for each class. Our analyses here have been motivated by the previous work of *Farquharson et al*. [1992] who carried out comparative analyses of similar dimensionless growth curves in catchments around the world and showed that they organize themselves into distinct growth curves on the basis of climate, although in their work climate was characterized qualitatively and not quantified in terms of the aridity index, *AI*.

The resulting growth curves, shown in Figure 5a, are indeed distinct for each aridity class. Overall, the growth curves for the high *AI* groups are steeper, with their concavity increasing with aridity. In other words, at high return periods, the scaled flood magnitudes are much higher for arid catchments than humid ones, and vice versa at low return periods (the mean being the same for all growth curves, due to the scaling by the respective mean annual floods). We repeated the analysis for flood frequency curves obtained for both surface flow and subsurface flow, and found almost identical results (for brevity, these results are not presented here). Before we can attribute these variations to annual water balance, we must discount the

© 2014. American Geophysical Union. All Rights Reserved.

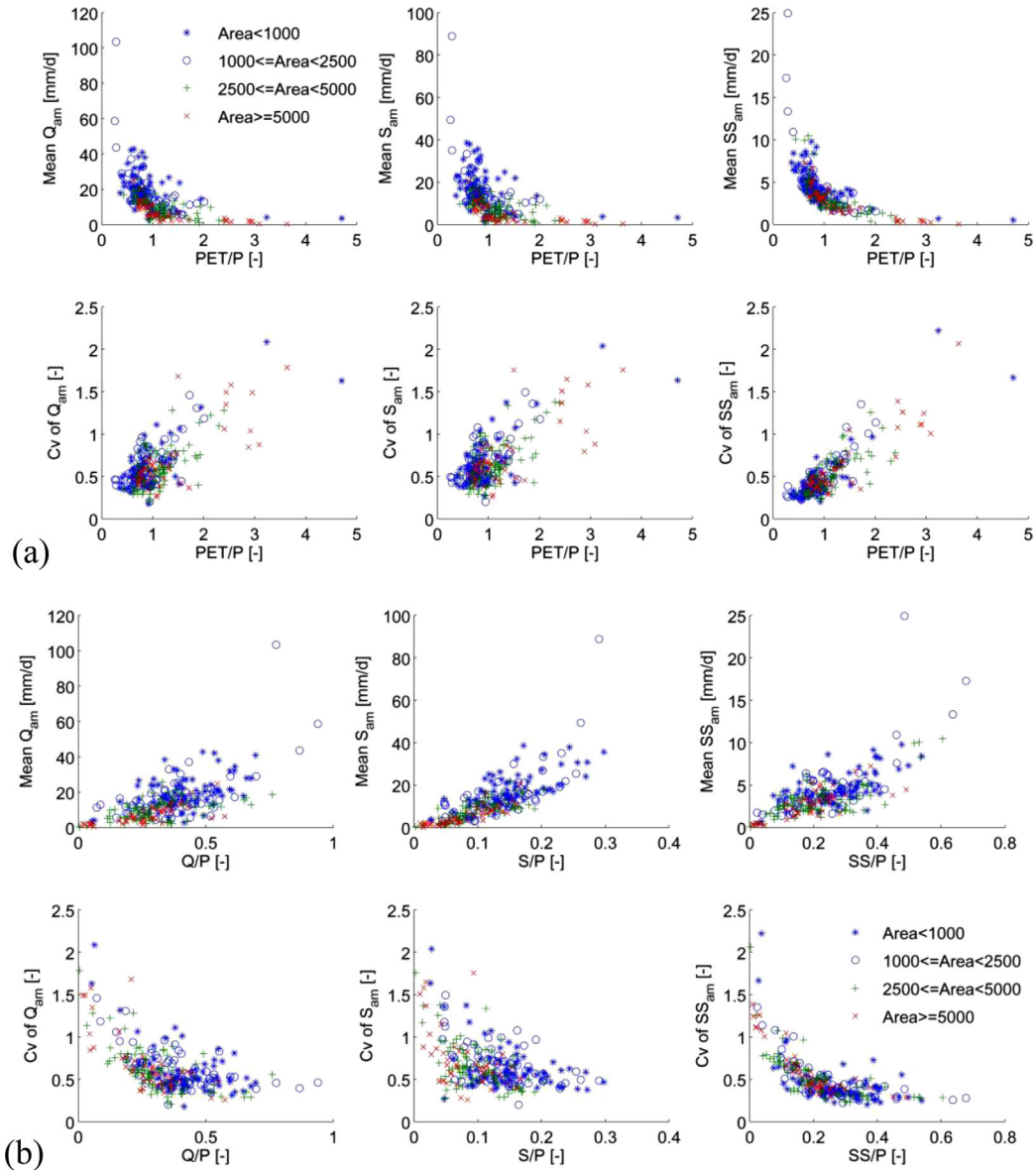

Figure 4. Statistical moments (Mean and C_v) of annual maximum of daily streamflow, Q_{am}, surface flow, S_{am}, subsurface flow, SS_{am} plotted against the (a) aridity index (*AI*) and (b) annual runoff ratio. The 266 MOPEX basins are divided into four groups according to their basin sizes: Area $<$ 1000 km^2, 1000 km^2 $\leq$ Area $<$ 2500 km^2, 2500 km^2 $\leq$ Area $<$ 5000 km^2, and Area $\geq$ 5000 km^2.

possibility that they may be simply due to differences in extreme precipitation. For this reason, we also constructed the corresponding (scaled) frequency curves for annual maximum 24 h (daily) precipitation, using the precipitation data available within the MOPEX data set. The results are presented in Figure 5b: they

Table 1. The Nonlinear (for Mean) and Linear (for C_v) Regression Relationships for Mean and C_v as a Function of *AI*, Derived for the Results Presented in Figure 4

	Ln (mean of ∼)	C_v of ∼
Q_{am}	-1.404 Ln(*AI*) + 2.298 ($R^2 = 0.542$) *p* value = 0.0000	0.2385 + 0.3615 *AI* ($R^2 = 0.506$) *p* value = 0.0000
S_{am}	-1.425 Ln(*AI*) + 2.065 ($R^2 = 0.453$) *p* value = 0.0000	0.2994 + 0.3513 *AI* ($R^2 = 0.459$) *p* value = 0.0000
SS_{am}	-1.441 Ln(*AI*) + 1.075 ($R^2 = 0.761$) *p* value = 0.0000	0.0708 + 0.4125 *AI* ($R^2 = 0.713$) *p* value = 0.0000
	Log (Mean ∼)	Log (C_v of ∼)
Q_{am}	3.41 + 0.89 Ln(*Q/P*) ($R^2 = 0.457$) *p* value = 0.0000	$-1.05 - 0.41$ Ln(*Q/P*) ($R^2 = 0.415$) *p* value = 0.0000
S_{am}	4.91 + 1.21 Ln(*S/P*) ($R^2 = 0.698$) *p* value = 0.0000	$-1.17 - 0.30$ Ln(*S/P*) ($R^2 = 0.249$) *p* value = 0.0000
SS_{am}	2.44 + 0.79 Ln(*SS/P*) ($R^2 = 0.643$) *p* value = 0.0000	$-1.57 - 0.48$ Ln(*SS/P*) ($R^2 = 0.671$) *p* value = 0.0000

© 2014. American Geophysical Union. All Rights Reserved.

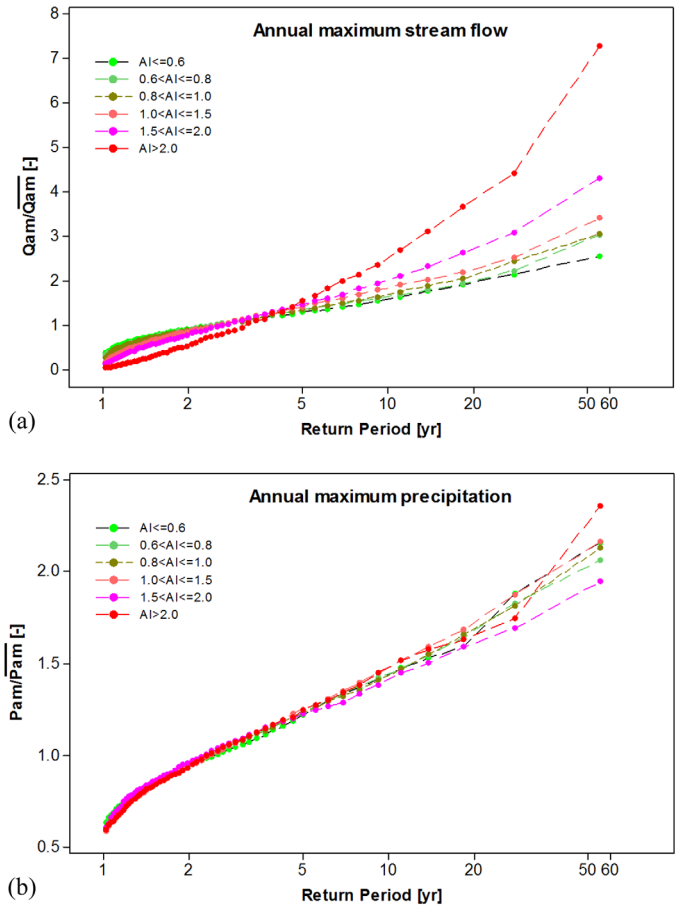

Figure 5. (a) Normalized growth curves for annual maximum streamflow, Q_{am}, and (b) annual maximum precipitation, P_{am}, for different classes of aridity index, *AI*. The flood frequency curve at an individual catchment is first normalized by dividing the annual maximum flood by the mean. Each regional curve in the figure is then derived by arithmetic averaging of the dimensionless floods for the same return period among basins belonging to a given aridity class.

show that there is much less variation between the six catchment classes, indicating strongly that the divergence between the annual maximum rainfall and flood frequency growth curves, and the differences between the different catchment classes, must arise due to nonlinearity in the transformation between precipitation and streamflow, not just at the event scale, but possibly across all the time scales of variability that contribute to annual water balance. Figure 5 shows that the assumption of similarity within each aridity index holds across a variety of climate and landscape properties. This indicates that *AI* could be a useful indicator for use in the regionalization of flood frequency curve. A more complete demonstration of this will requires detailed investigation of other landscape characteristic such as soil properties, topographic slope, vegetation cover, etc. and is beyond the scope of this paper and left for a future study.

Farquharson et al. [1992] suggested that the main causes for floods in arid areas are high-intensity storms but with relatively limited spatial extents and short durations, where rainfall rates exceed infiltration capacity at least within parts of a catchment. *Osterkamp and Friedman* [2000] reported that annual maximum flood peaks, flash-flood potentials, and runoff potentials are generally greater in semiarid areas than in more humid parts of the United States. *Osterkamp and Friedman* [2000] attributed the disparity between flood peaks and rainfall to the fact that, in humid regions, soil and vegetation absorb and intercept rainfall and attenuate runoff, while in semiarid regions the bare, crusted surfaces limit infiltration and enhance runoff. *Viglione et al.* [2009] pointed out that in a wet catchment where runoff coefficients are usually high, the return periods of floods are no more than a few times that of the corresponding rainfall events, whereas in a dry catchment where runoff events with high runoff coefficients are rarely observed, one event with high runoff coefficient can yield a flood with return period that is hundreds of times the return period of the corresponding rainfall event. Clearly, the connection between precipitation and flood frequency is complex, and highly nonlinear with increasing aridity, and will be further explored in subsequent sections.

3.3. Relationship Between BFI and Flood Frequency

Although the results presented in Figures 3–5 showed a clear dependence of flood frequency statistics on annual water balance through the aridity index, there was still considerable scatter in the relationships. This suggests that there may be other factors that contribute to the regional patterns of the flood frequency curve. We therefore next explore possible connections to the second water balance indicator, namely the base flow index (*BFI*), which may be more of an indicator of catchment physical characteristics rather than climate alone. Figure 6 presents the spatial distribution of *BFI* values for the 266 MOPEX basins. The spatial

© 2014. American Geophysical Union. All Rights Reserved.

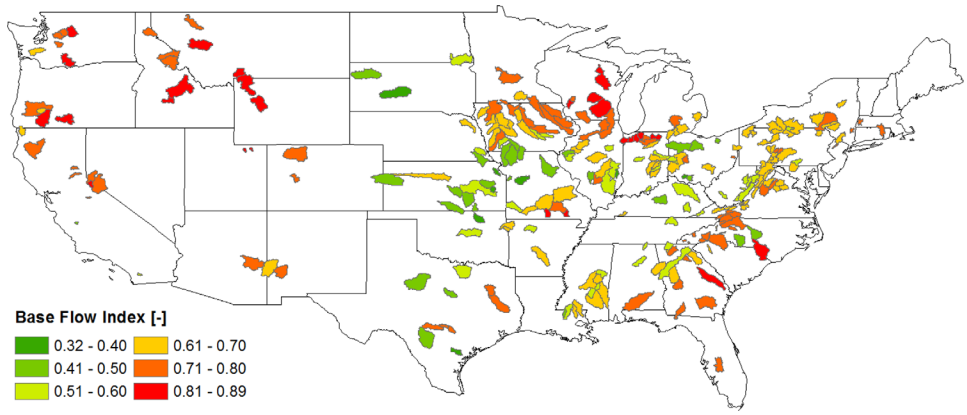

Figure 6. Spatial distribution of base flow index (*BFI*) over the 266 MOPEX basins.

pattern is not as spatially coherent as *AI* was in Figure 3c, which confirms that *BFI* reflects local rather than regional landscape features.

Figure 7a presents the ratio of mean annual maximum daily precipitation to mean annual maximum flood ($\bar{P}_{am}/\bar{Q}_{am}$) plotted against aridity index *AI* for the six *BFI* classes, while Figure 7b presents the corresponding relationship between the ratio of C_v *of* annual maximum daily precipitation to C_v of *AMF* (C_{vp}/C_{vq}) and the aridity index. Together they reveal the nature of the transformation between the annual maximum daily precipitation and annual maximum flood, in the frequency (return period) domain. In general, due to the space/time filtering of the catchment, one would expect the $\bar{P}_{am}/\bar{Q}_{am}$ ratio to be greater than unity, and the C_{vp}/C_{vq} ratio to be less than unity. Figure 7a shows that the ratio of the means (annual maximum precipitation to annual maximum flood) increases with increasing aridity, fairly tightly up to an aridity (*AI*) of about 1.25 and most *BFI* values; indeed, for the highest *BFI* values ($BFI > 0.8$), the ratio of the means appears to remain constant at close to a value of 1.0. At higher aridity values, however, the results for the ratio of means show greater diversity (and scatter), which cannot be attributed to differences of *BFI* values. The results for the C_{vp}/C_{vq} ratio presented in Figure 7b show more scatter than expected, especially for catchments with high *BFI* values (outliers located outside the envelopes); however, if the catchments with high *BFI* values are

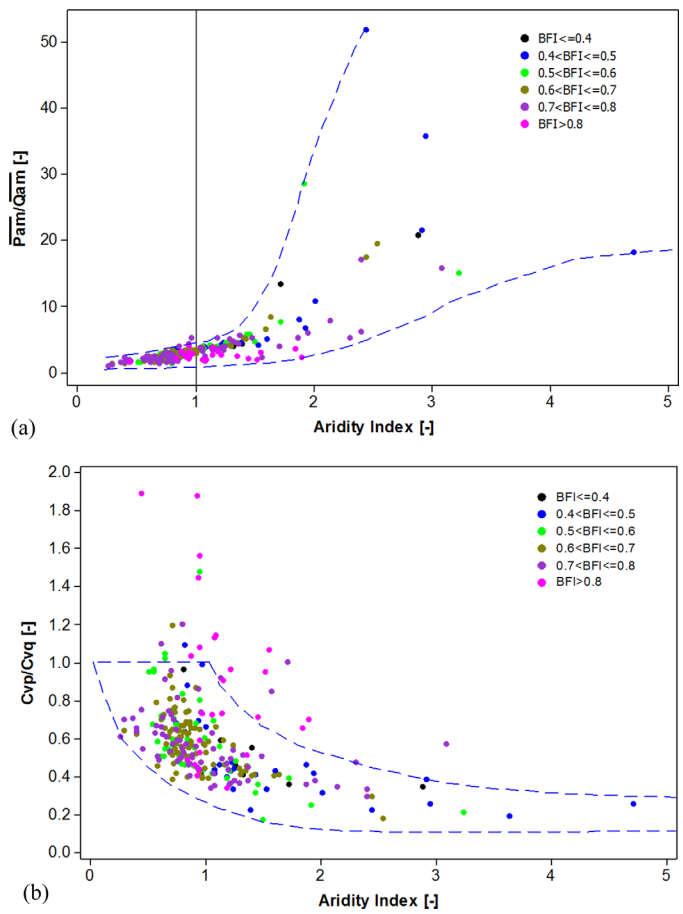

Figure 7. (a) $\bar{P}_{am}/\bar{Q}_{am}$, the ratio of mean and (b) C_{vp}/C_{vq}, the ratio of steepness of the annual maximum precipitation and annual maximum streamflow plotted against the aridity index (*AI*). The 266 MOPEX basins are divided into six classes according to the base flow index: $BFI \leq 0.4$, $0.4 < BFI \leq 0.5$, $0.5 < BFI \leq 0.6$, $0.6 < BFI \leq 0.7$, $0.7 < BFI \leq 0.8$, and $BFI > 0.8$.

© 2014. American Geophysical Union. All Rights Reserved.

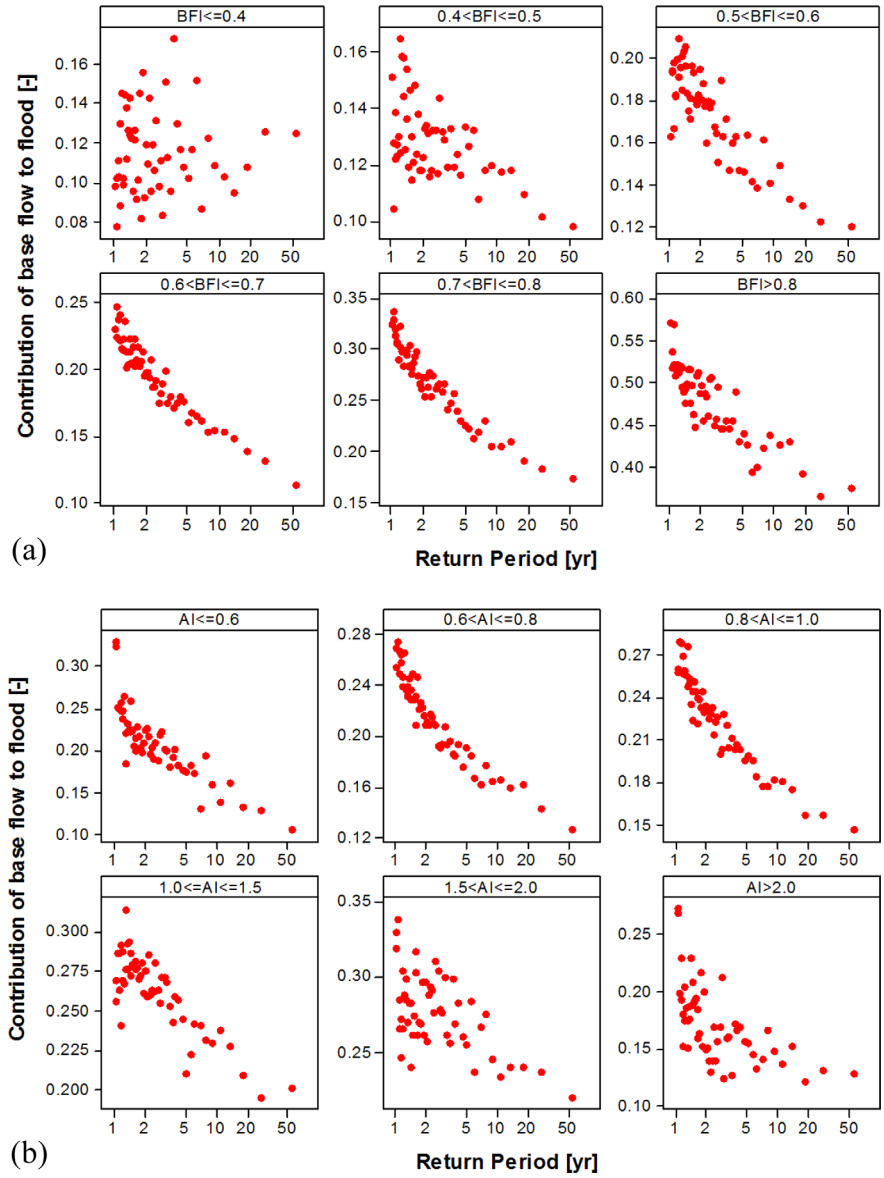

Figure 8. The contribution of base flow to annual maximum flood against return period for different (a) *BFI* group and (b) *AI* group. The contribution is defined as the ratio of base flow to streamflow on the day of the flood peak averaged over catchments within the same *BFI* or *AI* group. The MOPEX basins are divided into four groups according to *BFI*: (a) $BFI \leq 0.4$, $0.4 < BFI \leq 0.5$, $0.5 < BFI \leq 0.6$, $0.6 < BFI \leq 0.7$, $0.7 < BFI \leq 0.8$, $BFI > 0.8$ and according *AI*: (b) $AI \leq 0.6$, $0.6 < AI \leq 0.8$, $0.8 < AI \leq 1.0$, $1.0 < AI \leq 1.5$, $1.5 < AI \leq 2.0$, $AI > 2.0$.

removed (i.e., *BFI* values greater than 0.7), the remainder of the catchments do behave as expected, with the C_{vp}/C_{vq} ratio decreasing with increasing aridity, from a value close to unity for humid catchments and decreasing with increasing aridity. The physical causes of these patterns and discrepancies require further analysis. A clue that points to a possible explanation is that the problem catchments with high *BFI* values are either strongly snow dominated or vegetation (phenology) dominated [also see *Ye et al.*, 2012], which points to the influence of seasonality.

Additional insights into the patterns presented in Figures 4–7 can be gained by carrying out diagnostic studies on the relative contributions of fast and slow runoff to the recorded annual maximum flood peaks. This is relatively easy to determine, given the outcomes of the base flow separation done on the MOPEX data set. Once the annual maximum flood peak is determined for each year, given its timing, we can identify for the day of the annual maximum flood the relative magnitudes of *S* and *SS* and determine if the relative contributions change systematically with increasing return period. The results of this analysis for all 266 catchments are presented in Figure 8, organized in two different ways. Figure 8a shows the variation of the

© 2014. American Geophysical Union. All Rights Reserved.

Table 2. Results of Significant Tests for the Relationships Presented in Figure 8

	$BFI \leq 0.4$	$0.4 < BFI \leq 0.5$	$0.5 < BFI \leq 0.6$	$0.6 < BFI \leq 0.7$	$0.7 < BFI \leq 0.8$	$BFI > 0.8$
R^2	0.0007	0.298	0.742	0.898	0.891	0.759
p value	0.8456	0.0000	0.0000	0.0000	0.0000	0.0000
	$AI \leq 0.6$	$0.6 < AI \leq 0.8$	$0.8 < AI \leq 1.0$	$1.0 \leq AI \leq 1.5$	$1.5 < AI \leq 2.0$	$AI > 2.0$
R^2	0.7155	0.862	0.882	0.714	0.357	0.356
p value	0.0000	0.0000	0.0000	0.0000	0.0000	0.0000

fractional contributions of slow flow, *SS*, for the six different *AI* classes, going from humid to arid. Figure 8b shows the corresponding results for six different *BFI* classes, going from small *BFI* ($BFI < 0.4$) to large *BFI* ($BFI > 0.8$). We found no significant relationship between *AI* and *BFI* (figure not shown). In terms of the role of *AI*, the results show that for all six classes the slow flow fraction decreases from about 30% to about 10% with increasing return period (i.e., on average there are no substantial differences between the different *AI* classes). Therefore, the decrease of the *mean MAF* and increase of C_v with return period must be due to changes in the nonlinearity in the rainfall-runoff-flood peak transformation with increase of rainfall extremes, and not due to an increase in the fraction of surface runoff. On the other hand, in the case of the *BFI*, the increase of *BFI*, on average, leads to an increase in the fraction of subsurface flow *SS*, from only about 10% for $BFI < 0.4$ to about 50% for $BFI > 0.8$. The increasing subsurface component with increasing *BFI* means the nonlinearity associated with increasing rainfall extremes is not so strong, and therefore C_v decreases. The significance test results of these relationships are provided in Table 2. One can see that most of them are indeed statistically significant except for the case when *BFI* is no larger than 0.4. These results point to two ways that the *BFI* impacts on the flood frequency curve: (a) high values of *BFI* mean a dominance of subsurface flow contribution to the flood peak, which reduces both the *mean* and C_v and (b) low and intermediate values of the *BFI* mean a higher nonlinearity and relative independence of the precipitation peak and flood peak, and hence more scatter in the flood frequency statistics. The possible causes of these factors are explored next.

All of the results so far, taken together, indicate a strong but complex relationship between flood frequency and mean annual water balance. Not only the mean annual water balance (as governed by the *AI* and *BFI* indices), but also the relative timing of the fast (surface) and slow (subsurface) flow contributions to the annual maximum flood peak contribute to the shape of the resulting flood frequency curve. We now present results of further diagnostic analyses carried out with the MOPEX data set to get a deeper understanding of these connections.

From the MOPEX data set, for every catchment and for every year, we identify the annual (daily) maximum of precipitation (P_{am}), total streamflow (Q_{am}), surface flow (S_{am}), and subsurface flow (SS_{am}). In addition, from available *hourly* precipitation data associated with the annual maximum flood (Q_{am}), we derived event rainfall duration (*Tr*), event rainfall intensity (*Int*), and event rainfall depth (*Dep*) for each of the catchments and for each year. We then explored the association of Q_{am} with the other explanatory variables. The results are presented in Figure 9. The vertical axis in Figure 9 is the fraction of years (expressed in percentage terms) averaged over the 266 MOPEX basins that the annual daily maximum P_{am} (or S_{am}, SS_{am}, *Tr, Int*, and *Dep*) occurs *x* days $(x=0, 1, 2, \cdots, 10)$ before the annual maximum Q_{am} (*x* is the horizontal axis in Figure 9). Taking P_{am} as an example, the ratio corresponding to an *x* day window is calculated as

$$\alpha_{x,P_{am}} = \sum_{j=1}^{j=M} \frac{n_{x,j,P_{am}}}{N} / M \tag{8}$$

where $n_{x,j,P_{am}}$ is, for the *j*th basin, the number of years when the *AMF* (Q_{am}) occurred no later than the *x*th day after P_{am}, *M* is the total number of MOPEX basins, and *N* is the total number of years. Figure 9 presents the results for P_{am}, S_{am}, SS_{am}, *Tr, Int*, and *Dep*.

The results in Figure 9 show that on average, the chance that *AMF* (Q_{am}) occurs on the same day as annual maximum precipitation (P_{am}) is very low. In fact the chance that Q_{am} occurs even 5 days or more after P_{am} remains below 35%, suggesting that it is not P_{am} that normally leads to Q_{am} in any given year. Similarly, the chance for Q_{am} to be associated with *Tr* or *Int* is no more than 20% for the population of MOPEX catchments considered. On the other hand, on average, in about 75% of the

© 2014. American Geophysical Union. All Rights Reserved.

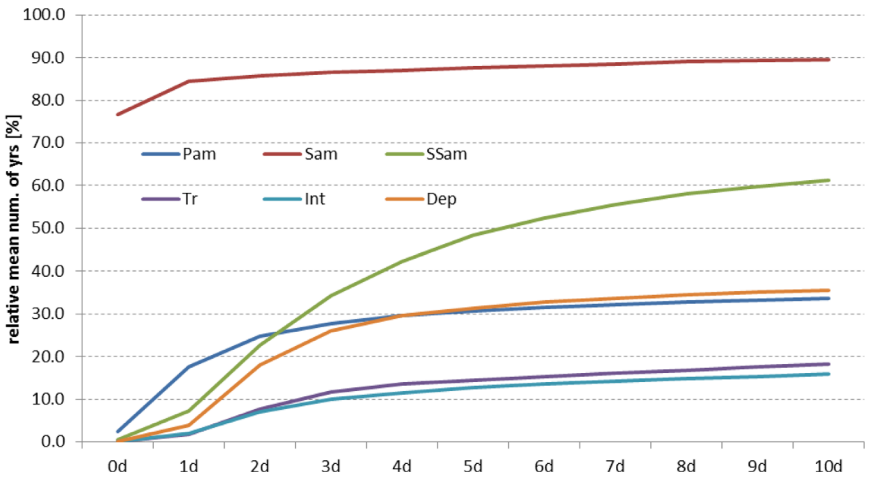

Figure 9. The probability that annual maximum flood occurs after a certain time of the occurrence of annual maximum daily precipitation (P_{am}), maximum surface flow (S_{am}), maximum subsurface flow (SS_{am}), maximum event rainfall duration (*Tr*), maximum event rainfall intensity (*Int*), and maximum event rainfall total depth (*Dep*). The probability is calculated as the fraction of years for each basin then averaged over the 266 MOPEX basins.

years, S_{am} is found to occur on the same day as Q_{am}, and the chance for Q_{am} to occur within 5 or more days after S_{am} hits close to 90%. One can thus say that Q_{am} is closely associated with S_{am}. On the other hand, SS_{am} rarely happens on the same day as the annual maximum flood, but the chance that Q_{am} occurs 5 days or more after SS_{am} is close to 50% and this number continues to increase as we wait longer. This means that the *AMF* in any year could be caused by a combination of a wet antecedent soil moisture condition and even medium-sized rainfall event. This is because SS_{am}, even if it occurred a few days earlier indicates that the soil has been sufficiently wet, remains wet and with the onset of a new rainfall event may lead to significant saturation excess runoff and/or fast subsurface runoff. The strong correlation between SS_{am} and Q_{am} suggests that antecedent soil moisture plays an important role in the generation of Q_{am} within the MOPEX catchments.

We can see from Figure 9 that the fraction of catchments on the vertical axis (which represents a probability) becomes stable after 5 days for most of the variables except for SS_{am}, which tends to have longer memory and more lasting effects. On the basis of this we chose 5 days as the cutoff for further analysis. Figure 10 shows, this time for each MOPEX basin, the fraction of time (i.e., percentage of years) that the annual maximum P_{am}, S_{am}, and SS_{am} occur 0–5 days before Q_{am} occurred. In the case of P_{am} (Figure 10a), there is an obvious spatial pattern: along the mountainous west coast and along the Appalachian Mountains the percentage of years is 40–60% whilst everywhere else the number is mostly less than 40%. This suggests that in rain-dominated regions or rain-to-snow transition (e.g., mountainous) regions where orography enhances rainfall, Q_{am} coincides more often with P_{am}. In snow-dominated mountains such as along the Rockies, and in the northern latitudes, the chance for Q_{am} and P_{am} to coincide is relatively low because Q_{am} may be more driven by snowmelt.

For S_{am} (Figure 10b), most of the catchments show percentages larger than 80%, meaning that Q_{am} is strongly associated with S_{am} everywhere. For SS_{am} (Figure 10c), however, there is considerable diversity in the results. In some catchments, the probability is as high as 60∼80% which means that the timing of flood peak is likely dominated by the timing of subsurface flow. It is interesting to compare Figures 6 and 10c to see that the spatial patterns of both *BFI* and the chance of SS_{am} occurring 0–5 days before Q_{am} are inversely related: where *BFI* is large, the chance of SS_{am} occurring 0–5 days before Q_{am} is low, suggesting that there is less chance for SS_{am} to coincide with Q_{am} when annual *BFI* is high. This may be because catchments with higher *BFI* values are more permeable, so it is easier for rainfall to infiltrate and enhance the peak of base flow. This means SS_{am} can happen at any time of the year but it may or may not contribute to Q_{am} occurring 0–5 days later. The huge difference between Figures 10a and 10b also show that even though surface flow is the quick response to precipitation, S_{am} is not necessarily (or not often) caused by P_{am}; instead, other factors such as antecedent soil moisture may play a more important role in contributing to the annual maximum flood peak.

© 2014. American Geophysical Union. All Rights Reserved.

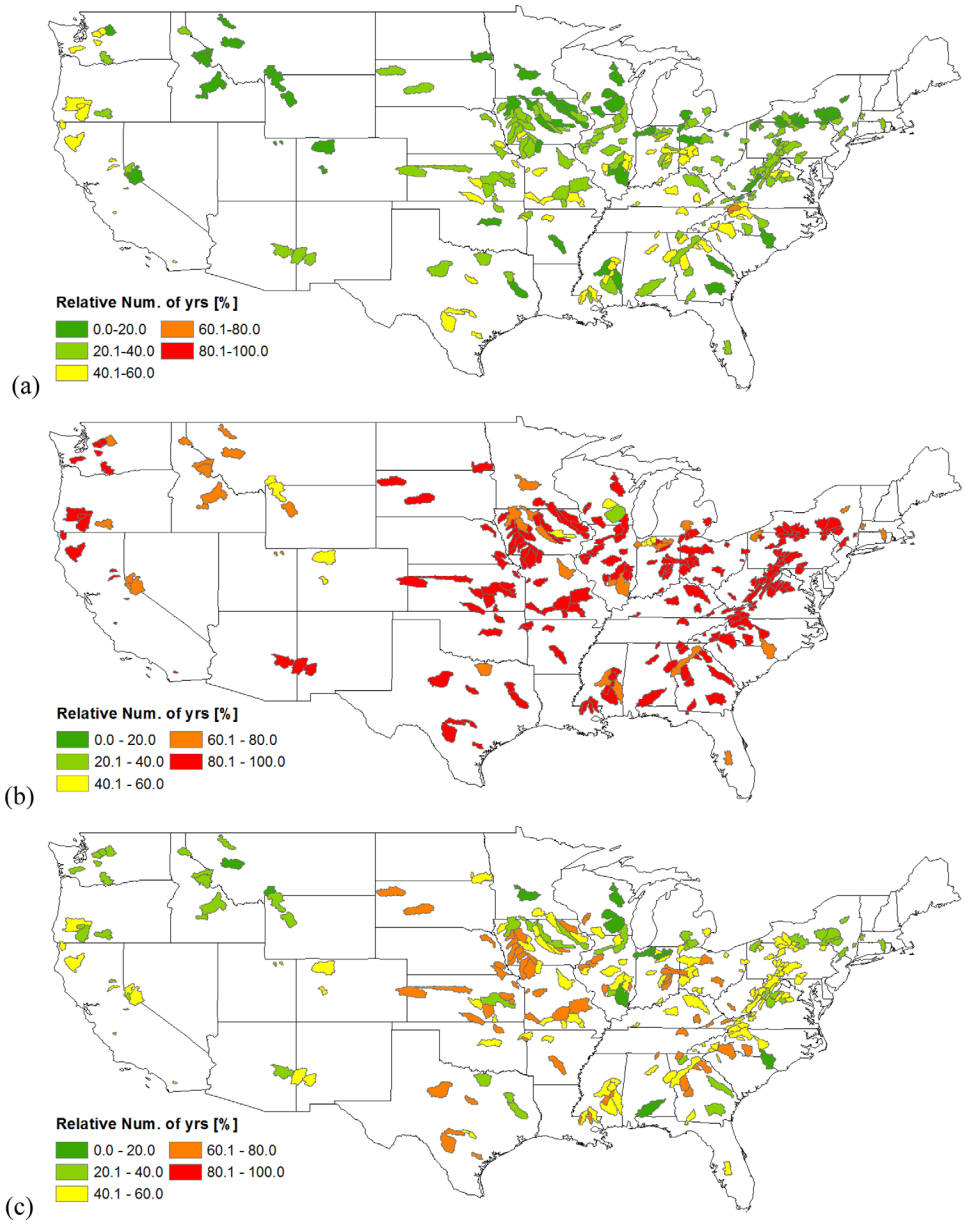

Figure 10. The relative number of years that (a) P_{am}, (b) S_{am}, and (c) SS_{am} occurs 0∼5 days ahead of Q_{am} during the period of 1948–2003.

The role of *BFI* on flood frequency can be explained in terms of the interplay between storm duration, t_r, and catchment residence time, t_c [*Robinson and Sivapalan*, 1997b]: when t_c is large relative to t_r (poorly drained catchments, leading to low *BFI*), then storage remains high between events and the flood peak may result from several events acting together. When t_c is small relative to t_r (well-drained catchments, leading to high *BFI*), there could be more subsurface flow, which may be delayed, but there is less chance for events to interact and amplify the response, so the resulting flood magnitudes tend to be lower. *Robinson and Sivapalan* [1997b] came up with a classification of flood regimes on the basis of ratios of time scales that can explain the behavior observed in the MOPEX catchments. They also speculated that the presence of seasonality between precipitation and potential evaporation, especially of the out-of-phase kind, will exacerbate this further, by creating more chances for storage to accumulate and contributing to larger floods.

Figure 11 shows the regression lines between the mean annual maximum daily total streamflow with the mean annual maximum daily surface and subsurface flows, respectively, based on the observed data from the MOPEX basins. For all the 266 MOPEX basins, the mean annual maximum of streamflow shows a single

© 2014. American Geophysical Union. All Rights Reserved.

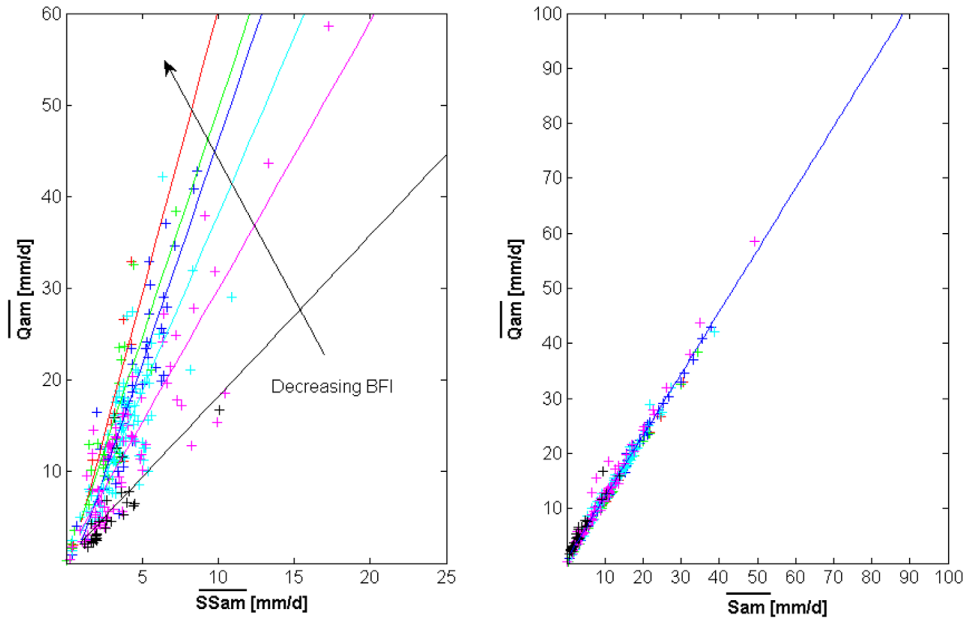

Figure 11. The relationship between mean annual flood ($\overline{Q_{am}}$) and mean annual maximum of the two runoff components ($\overline{SS_{am}}$ and $\overline{S_{am}}$).

compact relationship with the mean annual maximum of surface flow (Figure 11, right). On the other hand, the relationship between SS_{am} and Q_{am} is much more widespread, and seem to organize along the *BFI* groups (Figure 11, left). We see that with increasing *BFI*, the slope of the SS_{am} versus Q_{am} relationship decreases. This means for a specific mean annual maximum subsurface flow, the smaller BFI is, the larger the annual maximum flood is likely to be. For example, as *BFI* approaches zero, most flood peaks are likely to be caused by surface flow, and mean annual maximum daily subsurface flow also approaches zero. In contrast, when *BFI* approaches one, more flood peaks may be caused by subsurface flow, and the mean annual maximum subsurface flow gets close to the 1:1 line. In summary, Figures 9–11 show the close relationship between *AMF* and surface and subsurface runoff components, which is consistent with the Figures 4–7 that dealt with connection between flood frequency and annual water balance (as governed by *AI* and *BFI*).

4. Conclusions

This paper has presented the results of a data-based comparative study of several hundred catchments across continental United States to systematically explore the connection between the flood frequency curve and measures of mean annual water balance. The data used in this study is from 266 catchments that are a subset of the MOPEX data set that has been the subject of several recent comparative studies of catchment runoff signatures. Both the flood frequency curve and the annual water balance indices are signatures of runoff variability, occurring at opposite ends of the spectrum of hydrologic variability, and the connection between these signatures are of enormous significance both scientifically and for practical applications.

Two different measures of mean annual water balance have been used here: a climatic aridity index, *AI*, which is a measure of the competition between water and energy availability at the annual scale and is now well known to predict, to first order, the annual water balance of catchments, as per the famous Budyko curve. The second measure is the base flow index, *BFI*, the ratio of slow runoff to total runoff also at the annual time scale, which is predominantly a measure of landscape control on a particular aspect of the annual water balance, reflecting the role of geology, soils, topography, and vegetation.

Results of the data analysis showed that the aridity index, *AI*, has a first-order control on both the *mean* and C_v of annual maximum floods. For example, mean annual flood decreases with increasing aridity, reflecting on average dry conditions increase losses and decrease volume of runoff generation. In addition, the results showed that C_v goes up with increasing aridity, which is a reflection of nonlinearity of flood processes in

© 2014. American Geophysical Union. All Rights Reserved.

arid catchments with increasing return period, related potentially to change of dominant runoff generation processes and the effects of antecedent soil moisture conditions.

The base flow index, *BFI*, appeared to have a second-order control on the magnitude and shape of the flood frequency curve. *BFI* impacts the flood frequency curve in two different ways. Higher *BFI*, meaning more subsurface flow and less surface flow generally leads to a decrease of mean annual flood. This is due to the stronger filtering accomplished through the longer and slower pathways that water has to travel in the subsurface. A lower *BFI*, on the other hand, implies a poorly draining catchment, leading to accumulation of soil moisture between events, and increased flood magnitudes as a consequence of multiple events. This is one mechanism for the strong nonlinearity of flooding processes with increasing return period, and a steepness of the flood frequency in arid catchments. The role of *BFI* on flood frequency can be further explained in terms of the interplay between storm duration, t_r, and catchment residence time, t_c.

The results presented in this paper are significant in the context of long standing efforts at flood frequency regionalization, aimed at estimating design floods in ungauged basins. By attributing regional variations of the flood frequency curve to the aridity index and the base flow index, they provide an alternative basis to delineate hydrologically homogeneous regions within which the flood frequency curves can be assumed to be similar. At another level, developing further understanding of the connection between annual water balance and flood frequency will be another building block toward developing comprehensive understanding of hydrologic variability and similarity in a holistic way at the catchment scale. The aridity index, *AI*, which characterizes the similarity of annual water balance, has been reported recently as being indicative of the coevolution of catchment climate, soil, vegetation, and topography. For example, *Wang and Wu* [2013] found empirical evidence of a tight linkage between *AI* and scaled drainage density in the MOPEX catchments. *Xu et al*. [2012] reported strong correlation between *AI* and the fraction of deep-rooted vegetation in several hundred Australian catchments. These provide the hope that such coevolution and codependence of climate, soil, vegetation, and topography may form the basis of a comprehensive framework for hydrologic similarity. The empirical links documented in this study between flood frequency and annual water balance behaviors may provide the justification toward developing such a similarity framework.

In spite of the considerable insights that have been gained in the course of this study, there are several limitations inherent to the results and conclusions of this study. First of all, there are likely to be differences between the FFCs estimated from the daily streamflow data (as in this study) compared to FFCs constructed on the basis of instantaneous flow data. If flood frequency regionalization is to benefit from the links to annual water balance, then some adjustments may be necessary to account for this. Second, the locations of MOPEX catchments used in this study are spatially nonuniform, and the results obtained here are unrepresentative of much western United States. Therefore, some caution must be exercised in the interpretation of the results. More importantly, the relationship between annual water balance and flood frequency, was weaker in arid regions, and much more variable. This requires much more detailed study focused on these arid regions. Finally, there is a limit to what can be learned without more detailed exploration of within-year variability of both water balance and flood frequency. It appears that much of the scatter in the relationship between annual water balance and flood frequency can be attributed to our inability to capture the intraannual variability. This will be addressed in future work.

Acknowledgments
This study was supported by the Office of Science of the U.S. Department of Energy as part of the Regional and Global Climate Modeling Program and Earth System Modeling Program. The Pacific Northwest National Laboratory is operated for DOE by Battelle Memorial Institute under contract DE-AC05-76RLO 1830.

References

Arnold, J. G., and P. M. Allen (1999), Automated methods for estimating baseflow and ground water recharge from streamflow records, *J. Am. Water Resour. Assoc.*, *35*(2), 411–424.

Arnold, J. G., P. M. Allen, R. Muttiah, and G. Bernhardt (1995), Automated base flow separation and recession analysis techniques, *Ground Water*, *33*(6), 1010–1018.

Bloomfield, J. P., D. J. Allen, and K. J. Griffiths (2009), Examining geological controls on baseflow index (BFI) using regression analysis: An illustration from the Thames Basin, UK, *J. Hydrol.*, *373*(1–2), 164–176.

Blöschl, G., and M. Sivapalan (1997), Process controls on regional flood frequency: Coefficient of variation and basin scale, *Water Resour. Res.*, *33*(12), 2967–2980.

Blöschl, G., M. Sivapalan, T. Wagener, A. Viglione, and H. Savenije (2013), *Runoff Prediction in Ungauged Basins: Synthesis Across Processes, Places and Scales*, Cambridge Univ. Press, Cambridge, U. K.

Budyko, M. I. (1974), *Climate and Life*, Academic, N. Y.

Duan, Q., et al. (2005), Model parameter estimation experiment (MOPEX): Overview and summary of the second and third workshop results, *J. Hydrol.*, *320*, 3–17.

Farquharson, F. A. K., J. R. Meigh, and J. V. Sutcliffe (1992), Regional flood frequency analysis in arid and semi-arid areas, *J. Hydrol.*, *138*(3–4), 487–501.

 © 2014. American Geophysical Union. All Rights Reserved.

Fuller, W. E. (1914), Flood flows, *Trans. Am. Soc. Civ. Eng.*, *77*(1), 564–617.
Gebert, W. A., M. J. Radloff, E. J. Considine, and J. L. Kennedy (2007), Use of streamflow data to estimate base flow/ground-water recharge for Wisconsin, *J. Am. Water Resour. Assoc.*, *43*(1), 220–236.
Haberlandt, U., B. Klöcking, V. Krysanova, and A. Becker (2001), Regionalisation of the base flow index from dynamically simulated flow components—A case study in the Elbe River Basin, *J. Hydrol.*, *248*(1), 35–53.
Lacey, G. C., and R. B. Grayson (1998), Relating baseflow to catchment properties in south-eastern Australia, *J. Hydrol.*, *204*(1–4), 231–250.
Leung, L. R., L. O. Mearns, F. Giorgi, and R. L. Wilby (2003), Regional climate research: Needs and opportunities, *Bull. Am. Meteorol. Soc.*, *84*(1), 89–95.
Longobardi, A., and P. Villani (2008), Baseflow index regionalization analysis in a mediterranean area and data scarcity context: Role of the catchment permeability index, *J. Hydrol.*, *355*(1–4), 63–75.
L'vovich, M. I. (1979), *World Water Resources and Their Future*, AGU, Washington, D. C.
Lyne, V., and M. Hollick (1979), Stochastic time-variable rainfall-runoff modelling, in *Hydrology and Water Resources Symposium*, pp. 89–92, Natl. Comm. on Hydrol. and Water Resour. of the Inst. of Eng., Perth.
Madsen, H., and D. Rosbjerg (1997), Generalized least squares and empirical bayes estimation in regional partial duration series index-flood modeling, *Water Resour. Res.*, *33*(4), 771–781.
Merz, R., and G. Blöschl (2008a), Process controls on the statistical flood moments—A data based analysis, *Hydrol. Processes*, *23*(5), 675–696.
Merz, R., and G. Blöschl (2008b), Flood frequency hydrology: 1. Temporal, spatial, and causal expansion of information, *Water Resour. Res.*, *44*, W08432, doi:10.1029/2007WR006744.
Merz, R., and G. Blöschl (2008c), Flood frequency hydrology: 2. Combining data evidence, *Water Resour. Res.*, *44*, W08433, doi:10.1029/2007WR006745.
Nathan, R., and T. McMahon (1990), Evaluation of automated techniques for base flow and recession analyses, *Water Resour. Res.*, *26*(7), 1465–1473.
Osterkamp, W., and J. Friedman (2000), The disparity between extreme rainfall events and rare floods—With emphasis on the semi-arid American West, *Hydrol. Processes*, *14*(16–17), 2817–2829.
Reed, D., D. Faulkner, A. Robson, H. Houghton-Carr, A. Bayliss, and I. o. Hydrology (1999), *Flood Estimation Handbook: Procedures for Flood Frequency Estimation*, Institute of Hydrology, Wallingford, U. K.
Robinson, J. S., and M. Sivapalan (1997a), An investigation into the physical causes of scaling and heterogeneity of regional flood frequency, *Water Resour. Res.*, *33*(5), 1045–1059.
Robinson, J. S., and M. Sivapalan (1997b), Temporal scales and hydrological regimes: Implications for flood frequency scaling, *Water Resour. Res.*, *33*(12), 2981–2999.
Rosbjerg, D., G. Bloschl, D. H. Burn, A. Castellarin, B. Croke, G. D. Baldassarre, and V. Iacobells (2013), Prediction of floods in ungauged basins, in *Runoff Prediction in Ungauged Basins: Synthesis Across Processes, Places and Scales*, edited by G. Bloschl et al., pp. 189–226, Cambridge Univ. Press, Cambridge, U. K.
Singh, V., S. Wang, and L. Zhang (2005), Frequency analysis of nonidentically distributed hydrologic flood data, *J. Hydrol.*, *307*(1), 175–195.
Sivapalan, M., E. F. Wood, and K. J. Beven (1990), On hydrologic similarity: 3. A dimensionless flood frequency model using a generalized geomorphologic unit hydrograph and partial area runoff generation, *Water Resour. Res.*, *26*(1), 43–58.
Sivapalan, M., G. Blöschl, R. Merz, and D. Gutknecht (2005), Linking flood frequency to long-term water balance: Incorporating effects of seasonality, *Water Resour. Res.*, *41*, W06012, doi:10.1029/2004WR003439.
Sivapalan, M., M. A. Yaeger, C. J. Harman, X. Xu, and P. A. Troch (2011), Functional model of water balance variability at the catchment scale: 1. Evidence of hydrologic similarity and space-time symmetry, *Water Resour. Res.*, *47*, W02522, doi:10.1029/2010WR009568.
Struthers, I., and M. Sivapalan (2007), A conceptual investigation of process controls upon flood frequency: Role of thresholds, *Hydrol. Earth Syst. Sci.*, *11*(4), 1405–1416.
Szilagyi, J., and M. B. Parlange (1998), Baseflow separation based on analytical solutions of the Boussinesq equation, *J. Hydrol.*, *204*(1), 251–260.
Tebaldi, C., B. H. Strauss, and C. E. Zervas (2012), Modelling sea level rise impacts on storm surges along US coasts, *Environ. Res. Lett.*, *7*(1), 014032, doi:10.1088/1748–9326/7/1/014032.
Viglione, A., R. Merz, and G. Blöschl (2009), On the role of the runoff coefficient in the mapping of rainfall to flood return periods, *Hydrol. Earth Syst. Sci.*, *13*(5), 577–593.
Viglione, A., R. Merz, J. L. Salinas, and G. Blöschl (2013), Flood frequency hydrology: 3. A Bayesian analysis, *Water Resour. Res.*, *49*, 675–692, doi:10.1029/2011WR010782.
Voepel, H., B. Ruddell, R. Schumer, P. A. Troch, P. D. Brooks, A. Neal, M. Durcik, and M. Sivapalan (2011), Quantifying the role of climate and landscape characteristics on hydrologic partitioning and vegetation response, *Water Resour. Res.*, *47*, W00J09, doi:10.1029/2010WR009944.
Wang, D., and L. Wu (2013), Similarity of climate control on base flow and perennial stream density in the Budyko framework, *Hydrol. Earth Syst. Sci.*, *17*(1), 315–324.
Wood, E. F. (1976), An analysis of the effects of parameter uncertainty in deterministic hydrologic models, *Water Resour. Res.*, *12*(5), 925–932.
Wood, E. F., and C. S. Hebson (1986), On hydrologic similarity: 1. Derivation of the dimensionless flood frequency curve, *Water Resour. Res.*, *22*(11), 1549–1554.
Xu, X., D. Yang, and M. Sivapalan (2012), Assessing the impact of climate variability on catchment water balance and vegetation cover, *Hydrol. Earth Syst. Sci.*, *16*(1), 43–58.
Ye, S., M. Yaeger, E. Coopersmith, L. Cheng, and M. Sivapalan (2012), Exploring the physical controls of regional patterns of flow duration curves—Part 2: Role of seasonality and associated process controls, *Hydrol. Earth Syst. Sci.(16)*, *4447–4465*.
Zaman, M. A., A. Rahman, and K. Haddad (2012), Regional flood frequency analysis in arid regions: A case study for Australia, *J. Hydrol.*, *475*, 74–83.

 © 2014. American Geophysical Union. All Rights Reserved.